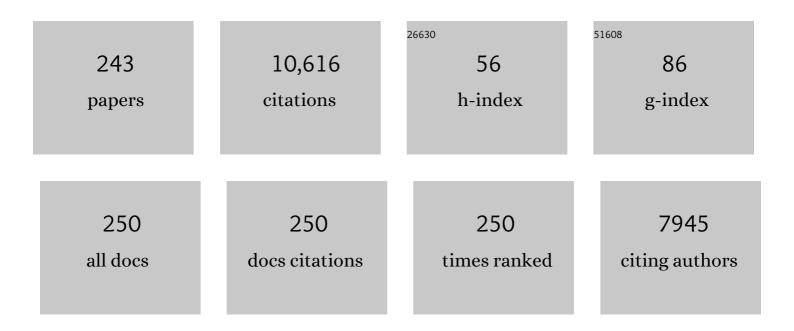
List of Publications by Year in descending order

Source: https://exaly.com/author-pdf/3576127/publications.pdf Version: 2024-02-01



 $linc_{i} \in (l_{i} \mid l_{i})$ 

#	Article	IF	CITATIONS
1	Shape-Dependent Electrocatalytic Reduction of CO <sub>2</sub> to CO on Triangular Silver Nanoplates. Journal of the American Chemical Society, 2017, 139, 2160-2163.	13.7	551
2	Recent Advances in MOFâ€Đerived Single Atom Catalysts for Electrochemical Applications. Advanced Energy Materials, 2020, 10, 2001561.	19.5	265
3	New Opportunity for <i>in Situ</i> Exsolution of Metallic Nanoparticles on Perovskite Parent. Nano Letters, 2016, 16, 5303-5309.	9.1	222
4	Anion Vacancies Regulating Endows MoSSe with Fast and Stable Potassium Ion Storage. ACS Nano, 2019, 13, 11843-11852.	14.6	210
5	Highly Stable and Efficient Catalyst with In Situ Exsolved Fe–Ni Alloy Nanospheres Socketed on an Oxygen Deficient Perovskite for Direct CO <sub>2</sub> Electrolysis. ACS Catalysis, 2016, 6, 6219-6228.	11.2	206
6	Boosting H <sub>2</sub> Generation Coupled with Selective Oxidation of Methanol into Valueâ€Added Chemical over Cobalt Hydroxide@Hydroxysulfide Nanosheets Electrocatalysts. Advanced Functional Materials, 2020, 30, 1909610.	14.9	190
7	A coupling for success: Controlled growth of Co/CoOx nanoshoots on perovskite mesoporous nanofibres as high-performance trifunctional electrocatalysts in alkaline condition. Nano Energy, 2017, 32, 247-254.	16.0	189
8	A-site deficient perovskite: the parent for in situ exsolution of highly active, regenerable nano-particles as SOFC anodes. Journal of Materials Chemistry A, 2015, 3, 11048-11056.	10.3	164
9	Progress in La-doped SrTiO <sub>3</sub> (LST)-based anode materials for solid oxide fuel cells. RSC Advances, 2014, 4, 118-131.	3.6	157
10	In situ facile fabrication of Ni(OH)2 nanosheet arrays for electrocatalytic co-production of formate and hydrogen from methanol in alkaline solution. Applied Catalysis B: Environmental, 2021, 281, 119510.	20.2	154
11	Coupling efficient biomass upgrading with H <sub>2</sub> production <i>via</i> bifunctional Cu <sub>x</sub> S@NiCo-LDH core–shell nanoarray electrocatalysts. Journal of Materials Chemistry A, 2020, 8, 1138-1146.	10.3	132
12	Allâ€Inâ€One Perovskite Catalyst: Smart Controls of Architecture and Composition toward Enhanced Oxygen/Hydrogen Evolution Reactions. Advanced Energy Materials, 2017, 7, 1700666.	19.5	124
13	Understanding the Roles of Electrogenerated Co <sup>3+</sup> and Co <sup>4+</sup> in Selectivity‶uned 5â€Hydroxymethylfurfural Oxidation. Angewandte Chemie - International Edition, 2021, 60, 20535-20542.	13.8	121
14	Development of electroless Ni–P/nano-WC composite coatings and investigation on its properties. Surface and Coatings Technology, 2015, 277, 99-106.	4.8	115
15	Ultrathin 5-fold twinned sub-25 nm silver nanowires enable highly selective electroreduction of CO2 to CO. Nano Energy, 2018, 45, 456-462.	16.0	115
16	A-site-deficiency facilitated in situ growth of bimetallic Ni–Fe nano-alloys: a novel coking-tolerant fuel cell anode catalyst. Nanoscale, 2015, 7, 11173-11181.	5.6	107
17	CO <sub>2</sub> -to-CO conversion on layered perovskite with in situ exsolved Co–Fe alloy nanoparticles: an active and stable cathode for solid oxide electrolysis cells. Journal of Materials Chemistry A, 2016, 4, 17521-17528.	10.3	106
18	The Excellence of Both Worlds: Developing Effective Double Perovskite Oxide Catalyst of Oxygen Reduction Reaction for Room and Elevated Temperature Applications. Advanced Functional Materials, 2016, 26, 4106-4112.	14.9	106

#	Article	IF	CITATIONS
19	Novel layered solid oxide fuel cells with multiple-twinned Ni <sub>0.8</sub> Co <sub>0.2</sub> nanoparticles: the key to thermally independent CO <sub>2</sub> utilization and power-chemical cogeneration. Energy and Environmental Science, 2016, 9, 207-215.	30.8	103
20	Boosting formate production at high current density from CO2 electroreduction on defect-rich hierarchical mesoporous Bi/Bi2O3 junction nanosheets. Applied Catalysis B: Environmental, 2020, 271, 118957.	20.2	103
21	Highly Active and Redox-Stable Ce-Doped LaSrCrFeO-Based Cathode Catalyst for CO <sub>2</sub> SOECs. ACS Applied Materials & Interfaces, 2016, 8, 6457-6463.	8.0	101
22	Activating p-Blocking Centers in Perovskite for Efficient Water Splitting. CheM, 2018, 4, 2902-2916.	11.7	99
23	Enhancing Perovskite Electrocatalysis of Solid Oxide Cells Through Controlled Exsolution of Nanoparticles. ChemSusChem, 2017, 10, 3333-3341.	6.8	97
24	Wavy SnO2 catalyzed simultaneous reinforcement of carbon dioxide adsorption and activation towards electrochemical conversion of CO2 to HCOOH. Applied Catalysis B: Environmental, 2020, 261, 118243.	20.2	97
25	Double-Layered Perovskite Anode with <i>in Situ</i> Exsolution of a Co–Fe Alloy To Cogenerate Ethylene and Electricity in a Proton-Conducting Ethane Fuel Cell. ACS Catalysis, 2016, 6, 760-768.	11.2	95
26	Anodeâ€Engineered Protonic Ceramic Fuel Cell with Excellent Performance and Fuel Compatibility. Advanced Materials, 2016, 28, 8922-8926.	21.0	94
27	Stabilizing Double Perovskite for Effective Bifunctional Oxygen Electrocatalysis in Alkaline Conditions. Chemistry of Materials, 2017, 29, 6228-6237.	6.7	94
28	Constructing multifunctional â€~Nanoplatelet-on-Nanoarray' electrocatalyst with unprecedented activity towards novel selective organic oxidation reactions to boost hydrogen production. Applied Catalysis B: Environmental, 2020, 278, 119339.	20.2	93
29	<i>In situ</i> grown cobalt phosphide (CoP) on perovskite nanofibers as an optimized trifunctional electrocatalyst for Zn–air batteries and overall water splitting. Journal of Materials Chemistry A, 2019, 7, 26607-26617.	10.3	92
30	<i>In Situ</i> Exsolved Metal Nanoparticles: A Smart Approach for Optimization of Catalysts. Chemistry of Materials, 2020, 32, 5424-5441.	6.7	89
31	Valueâ€Added Formate Production from Selective Methanol Oxidation as Anodic Reaction to Enhance Electrochemical Hydrogen Cogeneration. ChemSusChem, 2020, 13, 914-921.	6.8	87
32	Pr <sub>2</sub> BaNiMnO <sub>7â^î^</sub> double-layered Ruddlesden–Popper perovskite oxides as efficient cathode electrocatalysts for low temperature proton conducting solid oxide fuel cells. Journal of Materials Chemistry A, 2020, 8, 7704-7712.	10.3	84
33	Hollow NiSe Nanocrystals Heterogenized with Carbon Nanotubes for Efficient Electrocatalytic Methanol Upgrading to Boost Hydrogen Coâ€Production. Advanced Functional Materials, 2021, 31, 2008812.	14.9	84
34	Co P@NiCo-LDH heteronanosheet arrays as efficient bifunctional electrocatalysts for co-generation of value-added formate and hydrogen with less-energy consumption. Journal of Energy Chemistry, 2020, 50, 314-323.	12.9	83
35	A strongly cooperative spinel nanohybrid as an efficient bifunctional oxygen electrocatalyst for oxygen reduction reaction and oxygen evolution reaction. Applied Catalysis B: Environmental, 2018, 236, 413-419.	20.2	82
36	A mechanistic study on thiosulfate-enhanced passivity degradation of Alloy 800 in chloride solutions. Electrochimica Acta, 2013, 111, 510-525.	5.2	81

#	Article	IF	CITATIONS
37	Unraveling Structure Sensitivity in CO <sub>2</sub> Electroreduction to Near-Unity CO on Silver Nanocubes. ACS Catalysis, 2020, 10, 3158-3163.	11.2	80
38	Electronic Delocalization of Bismuth Oxide Induced by Sulfur Doping for Efficient CO <sub>2</sub> Electroreduction to Formate. ACS Catalysis, 2021, 11, 7604-7612.	11.2	80
39	The excellence of La(Sr)Fe(Ni)O <sub>3</sub> as an active and efficient cathode for direct CO <sub>2</sub> electrochemical reduction at elevated temperatures. Journal of Materials Chemistry A, 2017, 5, 2673-2680.	10.3	78
40	Review—Electrochemical Noise Applied in Corrosion Science: Theoretical and Mathematical Models towards Quantitative Analysis. Journal of the Electrochemical Society, 2020, 167, 081507.	2.9	78
41	Rational Design of Silver Sulfide Nanowires for Efficient CO <sub>2</sub> Electroreduction in Ionic Liquid. ACS Catalysis, 2018, 8, 1469-1475.	11.2	76
42	CO2-emission-free electrocatalytic CH3OH selective upgrading with high productivity at large current densities for energy saved hydrogen co-generation. Nano Energy, 2021, 80, 105530.	16.0	76
43	Bifunctional Catalyst of Core–Shell Nanoparticles Socketed on Oxygen-Deficient Layered Perovskite for Soot Combustion: <i>In Situ</i> Observation of Synergistic Dual Active Sites. ACS Catalysis, 2016, 6, 2710-2714.	11.2	70
44	Correlation of Fuel Cell Anode Electrocatalytic and ex situ Catalytic Activity of Perovskites La <sub>0.75</sub> Sr <sub>0.25</sub> Cr <sub>0.5</sub> X <sub>0.5</sub> O <sub>3â^Î</sub> (X = Ti, Mn, Fe,)	Tj <b>&amp;.7</b> Qq0	0 @ <b>s</b> gBT /Ove
45	Effects of hydrogen and stress on the electrochemical and passivation behaviour of 304 stainless steel in simulated PEMFC environment. Electrochimica Acta, 2019, 293, 60-77.	5.2	68
46	Reducing d-p band coupling to enhance CO2 electrocatalytic activity by Mg-doping in Sr2FeMoO6-δ double perovskite for high performance solid oxide electrolysis cells. Nano Energy, 2021, 82, 105707.	16.0	67
47	Bifunctional Pt–Co <sub>3</sub> O <sub>4</sub> electrocatalysts for simultaneous generation of hydrogen and formate <i>via</i> energy-saving alkaline seawater/methanol co-electrolysis. Journal of Materials Chemistry A, 2021, 9, 6316-6324.	10.3	65
48	Unraveling the effects of CO2 and H2S on the corrosion behavior of electroless Ni-P coating in CO2/H2S/Cl– environments at high temperature and high pressure. Corrosion Science, 2019, 148, 317-330.	6.6	63
49	Y-doped BaCeO3â <sup>~</sup> δ nanopowders as proton-conducting electrolyte materials for ethane fuel cells to co-generate ethylene and electricity. Journal of Power Sources, 2010, 195, 2659-2663.	7.8	62
50	Hierarchically assembling cobalt/nickel carbonate hydroxide on copper nitride nanowires for highly efficient water splitting. Applied Catalysis B: Environmental, 2021, 292, 120148.	20.2	62
51	Ultrasmall Bi nanoparticles confined in carbon nanosheets as highly active and durable catalysts for CO2 electroreduction. Applied Catalysis B: Environmental, 2021, 284, 119723.	20.2	61
52	A rational design for enhanced oxygen reduction: Strongly coupled silver nanoparticles and engineered perovskite nanofibers. Nano Energy, 2017, 38, 392-400.	16.0	60
53	Cogeneration of ethylene and energy in protonic fuel cell with an efficient and stable anode anchored with in-situ exsolved functional metal nanoparticles. Applied Catalysis B: Environmental, 2018, 220, 283-289.	20.2	60
54	Constructing novel cross-linked polybenzimidazole network for high-performance high-temperature proton exchange membrane. Journal of Membrane Science, 2022, 643, 120037.	8.2	60

#	Article	IF	CITATIONS
55	A study on corrosion behaviors of Ni–Cr–Mo laser coating, 316 stainless steel and X70 steel in simulated solutions with H2S and CO2. Surface and Coatings Technology, 2016, 291, 250-257.	4.8	57
56	Developing hierarchically porous MnO <sub>x</sub> /NC hybrid nanorods for oxygen reduction and evolution catalysis. Green Chemistry, 2017, 19, 2793-2797.	9.0	57
57	Effect of defect on corrosion behavior of electroless Ni-P coating in CO2-saturated NaCl solution. Corrosion Science, 2018, 134, 23-37.	6.6	57
58	Carbon nanofibers@NiSe core/sheath nanostructures as efficient electrocatalysts for integrating highly selective methanol conversion and less-energy intensive hydrogen production. Journal of Materials Chemistry A, 2019, 7, 25878-25886.	10.3	57
59	CO2 dry reforming of CH4 with Sr and Ni co-doped LaCrO3 perovskite catalysts. Applied Surface Science, 2020, 506, 144699.	6.1	57
60	Cobalt doped LaSrTiO3ⴴδ as an anode catalyst: effect of Co nanoparticle precipitation on SOFCs operating on H2S-containing hydrogen. Journal of Materials Chemistry A, 2013, 1, 9689.	10.3	56
61	Carbon-tolerant Ni-based cermet anodes modified by proton conducting yttrium- and ytterbium-doped barium cerates for direct methane solid oxide fuel cells. Journal of Materials Chemistry A, 2015, 3, 21609-21617.	10.3	56
62	A facile surface chemistry approach to bifunctional excellence for perovskite electrocatalysis. Nano Energy, 2018, 49, 117-125.	16.0	55
63	Corrosion and wear resistance of chrome white irons—A correlation to their composition and microstructure. Metallurgical and Materials Transactions A: Physical Metallurgy and Materials Science, 2006, 37, 3029-3038.	2.2	54
64	Enhancing Sulfur Tolerance of Ni-Based Cermet Anodes of Solid Oxide Fuel Cells by Ytterbium-Doped Barium Cerate Infiltration. ACS Applied Materials & Interfaces, 2016, 8, 10293-10301.	8.0	54
65	Interfaceâ€induced Electrocatalytic Enhancement of CO <sub>2</sub> â€toâ€Formate Conversion on Heterostructured Bismuthâ€Based Catalysts. Small, 2022, 18, e2105682.	10.0	53
66	Smart utilization of cobaltite-based double perovskite cathodes on barrier-layer-free zirconia electrolyte of solid oxide fuel cells. Journal of Materials Chemistry A, 2016, 4, 19019-19025.	10.3	51
67	Hexagonal Zn Nanoplates Enclosed by Zn(100) and Zn(002) Facets for Highly Selective CO <sub>2</sub> Electroreduction to CO. ACS Applied Materials & Interfaces, 2020, 12, 31431-31438.	8.0	51
68	Interfacial engineering of Cu2Se/Co3Se4 multivalent hetero-nanocrystals for energy-efficient electrocatalytic co-generation of value-added chemicals and hydrogen. Applied Catalysis B: Environmental, 2021, 285, 119800.	20.2	51
69	Constructing stable continuous proton transport channels by in-situ preparation of covalent triazine-based frameworks in phosphoric acid-doped polybenzimidazole for high-temperature proton exchange membranes. Journal of Membrane Science, 2021, 640, 119775.	8.2	51
70	Tuning adsorption strength of CO2 and its intermediates on tin oxide-based electrocatalyst for efficient CO2 reduction towards carbonaceous products. Applied Catalysis B: Environmental, 2020, 277, 119252.	20.2	50
71	Phosphoric acid-doped polybenzimidazole with a leaf-like three-layer porous structure as a high-temperature proton exchange membrane for fuel cells. Journal of Materials Chemistry A, 2021, 9, 26345-26353.	10.3	50
72	Ethane dehydrogenation over nano-Cr2O3 anode catalyst in proton ceramic fuel cell reactors to co-produce ethylene and electricity. Journal of Power Sources, 2011, 196, 1036-1041.	7.8	49

#	Article	IF	CITATIONS
73	A-site deficient chromite perovskite with in situ exsolution of nano-Fe: a promising bi-functional catalyst bridging the growth of CNTs and SOFCs. Journal of Materials Chemistry A, 2015, 3, 14625-14630.	10.3	49
74	Phase-field model of pitting corrosion kinetics in metallic materials. Npj Computational Materials, 2018, 4, .	8.7	49
75	Bi <sub>2</sub> O <sub>3</sub> Nanosheets Grown on Carbon Nanofiber with Inherent Hydrophobicity for High-Performance CO <sub>2</sub> Electroreduction in a Wide Potential Window. ACS Nano, 2021, 15, 17757-17768.	14.6	47
76	The evolution of hierarchical porosity in self-templated nitrogen-doped carbons and its effect on oxygen reduction electrocatalysis. RSC Advances, 2016, 6, 80398-80407.	3.6	46
77	Electrochemical Transformation of Facetâ€Controlled BiOI into Mesoporous Bismuth Nanosheets for Selective Electrocatalytic Reduction of CO <sub>2</sub> to Formic Acid. ChemSusChem, 2019, 12, 4700-4707.	6.8	46
78	Modeling the effect of insoluble corrosion products on pitting corrosion kinetics of metals. Npj Materials Degradation, 2019, 3, .	5.8	46
79	γ-MnO2 nanorod-assembled hierarchical micro-spheres with oxygen vacancies to enhance electrocatalytic performance toward the oxygen reduction reaction for aluminum-air batteries. Journal of Energy Chemistry, 2020, 51, 81-89.	12.9	45
80	Nanotubular surface modification of metallic implants via electrochemical anodization technique. International Journal of Nanomedicine, 2014, 9, 4421.	6.7	43
81	Toward Excellence of Electrocatalyst Design by Emerging Descriptorâ€Oriented Machine Learning. Advanced Functional Materials, 2022, 32, .	14.9	43
82	An ingenious Ni/Ce co-doped titanate based perovskite as a coking-tolerant anode material for direct hydrocarbon solid oxide fuel cells. Journal of Materials Chemistry A, 2015, 3, 22830-22838.	10.3	42
83	Fabrication and characterization of a tubular ceramic fuel cell based on BaZr0.1Ce0.7Y0.1Yb0.1O3-Î <sup>^</sup> proton conducting electrolyte. Journal of Power Sources, 2017, 341, 264-269.	7.8	42
84	Review—Factors Influencing Sulfur Induced Corrosion on the Secondary Side in Pressurized Water Reactors (PWRs). Journal of the Electrochemical Society, 2019, 166, C49-C64.	2.9	42
85	Descriptor of catalytic activity of metal sulfides for oxygen reduction reaction: a potential indicator for mineral flotation. Journal of Materials Chemistry A, 2018, 6, 9650-9656.	10.3	41
86	Electrolyte Driven Highly Selective CO <sub>2</sub> Electroreduction at Low Overpotentials. ACS Catalysis, 2019, 9, 10440-10447.	11.2	41
87	Sensing corrosion within an artificial defect in organic coating using SECM. Sensors and Actuators B: Chemical, 2019, 280, 235-242.	7.8	41
88	Metal-support interaction enhanced electrochemical reduction of CO2 to formate between graphene and Bi nanoparticles. Journal of CO2 Utilization, 2020, 37, 353-359.	6.8	41
89	UnravelingÂthe Enhanced Kinetics of Sr <sub>2</sub> Fe <sub>1+</sub> <i><sub>x</sub></i> Mo <sub>1â€</sub> <i><sub>x</sub>6â€ŕElectrocatalysts for Highâ€Performance Solid Oxide Cells. Advanced Energy Materials, 2021, 11, 2102845.</i>	su <b>b9.</b> 5	41
90	Sulfur-Tolerant Anode Catalyst for Solid Oxide Fuel Cells Operating on H2S-Containing Syngas. Chemistry of Materials, 2010, 22, 1032-1037.	6.7	40

#	Article	IF	CITATIONS
91	Hollow Porous Ag Spherical Catalysts for Highly Efficient and Selective Electrocatalytic Reduction of CO <sub>2</sub> to CO. ACS Sustainable Chemistry and Engineering, 2019, 7, 14443-14450.	6.7	40
92	Toward a rational photocatalyst design: a new formation strategy of co-catalyst/semiconductor heterostructures <i>via in situ</i> exsolution. Chemical Communications, 2018, 54, 1505-1508.	4.1	39
93	Gum Arabic as corrosion inhibitor in the oil industry: experimental and theoretical studies. Corrosion Engineering Science and Technology, 2019, 54, 444-454.	1.4	39
94	A High-Performance Ruddlesden–Popper Perovskite for Bifunctional Oxygen Electrocatalysis. ACS Catalysis, 2020, 10, 13437-13444.	11.2	39
95	Folic acid self-assembly synthesis of ultrathin N-doped carbon nanosheets with single-atom metal catalysts. Energy Storage Materials, 2021, 36, 409-416.	18.0	39
96	Folic Acid Self-Assembly Enabling Manganese Single-Atom Electrocatalyst for Selective Nitrogen Reduction to Ammonia. Nano-Micro Letters, 2021, 13, 125.	27.0	39
97	La0.5Sr0.5Fe0.9Mo0.1O3-Î <sup>-</sup> -CeO2 anode catalyst for Co-Producing electricity and ethylene from ethane in proton-conducting solid oxide fuel cells. Ceramics International, 2021, 47, 24106-24114.	4.8	39
98	pH Effect on Sulfur-Induced Passivity Degradation of Alloy 800 in Simulated Crevice Chemistries. Journal of the Electrochemical Society, 2014, 161, C201-C214.	2.9	38
99	Facile Preparation of Self-Standing Hierarchical Porous Nitrogen-Doped Carbon Fibers for Supercapacitors from Plant Protein–Lignin Electrospun Fibers. ACS Omega, 2018, 3, 4647-4656.	3.5	38
100	A-site deficient perovskite with nano-socketed Ni-Fe alloy particles as highly active and durable catalyst for high-temperature CO2 electrolysis. Electrochimica Acta, 2020, 335, 135683.	5.2	38
101	All roads lead to Rome: An energy-saving integrated electrocatalytic CO2 reduction system for concurrent value-added formate production. Chemical Engineering Journal, 2021, 412, 127893.	12.7	38
102	Combating marine corrosion on engineered oxide surface by repelling, blocking and capturing Clâ^': A mini review. Corrosion Communications, 2021, 2, 1-7.	6.0	38
103	Performance of Ethane/Oxygen Fuel Cells Using Yttrium-Doped Barium Cerate as Electrolyte at Intermediate Temperatures. Journal of Physical Chemistry C, 2007, 111, 5069-5074.	3.1	37
104	Alternative Fuel Cell Technologies for Cogenerating Electrical Power and Syngas from Greenhouse Gases. ACS Energy Letters, 2017, 2, 1789-1796.	17.4	37
105	Characterization of microstructure and properties of electroless duplex Ni-W-P/Ni-P nano-ZrO2 composite coating. Materials Today Physics, 2018, 4, 36-42.	6.0	37
106	Achieving ultrahigh corrosion resistance and conductive zirconium oxynitride coating on metal bipolar plates by plasma enhanced atomic layer deposition. Journal of Power Sources, 2018, 397, 32-36.	7.8	37
107	Multi-functionalities enabled fivefold applications of LaCo0.6Ni0.4O3â^î^ in intermediate temperature symmetrical solid oxide fuel/electrolysis cells. Nano Energy, 2020, 77, 105207.	16.0	37
108	Carbon Dioxide Valorization via Formate Electrosynthesis in a Wide Potential Window. Advanced Functional Materials, 2022, 32, .	14.9	37

#	Article	IF	CITATIONS
109	Sulfur induced corrosion (SIC) mechanism of steam generator (SC) tubing at micro scale: A critical review. Materials Chemistry and Physics, 2019, 233, 133-140.	4.0	36
110	Efficient bifunctional electrocatalysts for solid oxide cells based on the structural evolution of perovskites with abundant defects and exsolved CoFe nanoparticles. Journal of Power Sources, 2021, 482, 228981.	7.8	36
111	Ca-containing Ba0·95Ca0·05Co0·4Fe0·4Zr0·1Y0·1O3-Î′ cathode with high CO2-poisoning tolerance for proton-conducting solid oxide fuel cells. Journal of Power Sources, 2020, 453, 227909.	7.8	35
112	Tuning local carbon active sites saturability of graphitic carbon nitride to boost CO2 electroreduction towards CH4. Nano Energy, 2020, 73, 104833.	16.0	35
113	Electrochemical exfoliation from an industrial ingot: ultrathin metallic bismuth nanosheets for excellent CO <sub>2</sub> capture and electrocatalytic conversion. Nanoscale, 2019, 11, 22125-22133.	5.6	34
114	Protonic membrane for fuel cell for co-generation of power and ethylene. Journal of Power Sources, 2008, 176, 122-127.	7.8	31
115	An integral proton conducting SOFC for simultaneous production of ethylene and power from ethane. Chemical Communications, 2010, 46, 2052.	4.1	31
116	Understanding the interaction of thiosulfate with Alloy 800 in aqueous chloride solutions using SECM. Journal of Electroanalytical Chemistry, 2015, 744, 77-84.	3.8	31
117	Microwave-assisted hydrothermal synthesis of MOFs-derived bimetallic CuCo-N/C electrocatalyst for efficient oxygen reduction reaction. Journal of Alloys and Compounds, 2019, 795, 462-470.	5.5	31
118	Enhancing through-plane electrical conductivity by introducing Au microdots onto TiN coated metal bipolar plates of PEMFCs. International Journal of Hydrogen Energy, 2020, 45, 29442-29448.	7.1	31
119	In situ embedding of CoFe nanocatalysts into Sr3FeMoO7 matrix as high-performance anode materials for solid oxide fuel cells. Journal of Power Sources, 2020, 459, 228071.	7.8	31
120	Constructing proton transport channels in low phosphoric-acid doped polybenzimidazole membrane by introducing metal–organic frameworks containing phosphoric-acid groups. Journal of Power Sources, 2021, 507, 230316.	7.8	31
121	Semiconductivity conversion of Alloy 800 in sulphate, thiosulphate, and chloride solutions. Corrosion Science, 2014, 87, 265-277.	6.6	30
122	Biogas to syngas: flexible on-cell micro-reformer and NiSn bimetallic nanoparticle implanted solid oxide fuel cells for efficient energy conversion. Journal of Materials Chemistry A, 2016, 4, 4603-4609.	10.3	30
123	Carbon-resistant Ni-Zr0.92Y0.08O2-δ supported solid oxide fuel cells using Ni-Cu-Fe alloy cermet as on-cell reforming catalyst and mixed methane-steam as fuel. Journal of Power Sources, 2016, 303, 340-346.	7.8	30
124	<i>In situ</i> construction of hetero-structured perovskite composites with exsolved Fe and Cu metallic nanoparticles as efficient CO <sub>2</sub> reduction electrocatalysts for high performance solid oxide electrolysis cells. Journal of Materials Chemistry A, 2022, 10, 2509-2518.	10.3	30
125	Achieving Efficient CO <sub>2</sub> Electrochemical Reduction on Tunable In(OH) <sub>3</sub> -Coupled Cu <sub>2</sub> O-Derived Hybrid Catalysts. ACS Applied Materials & Interfaces, 2019, 11, 22346-22351.	8.0	28
126	A mechanistic study on sulfur-induced passivity degradation on Alloy 800 in simulated alkaline crevice chemistries at temperatures ranging from 21 °C to 300 °C. Corrosion Science, 2015, 100, 504-516.	6.6	27

#	Article	IF	CITATIONS
127	Facile Synthesis of Highly Active and Robust Ni–Mo Bimetallic Electrocatalyst for Hydrocarbon Oxidation in Solid Oxide Fuel Cells. ACS Energy Letters, 2016, 1, 225-230.	17.4	27
128	Grafting doped manganite into nickel anode enables efficient and durable energy conversions in biogas solid oxide fuel cells. Applied Catalysis B: Environmental, 2017, 200, 174-181.	20.2	27
129	Insights into the Interfacial Process in Electroless Ni–P Coating on Supercritical CO <sub>2</sub> Transport Pipeline as Relevant to Carbon Capture and Storage. ACS Applied Materials & Interfaces, 2019, 11, 16243-16251.	8.0	27
130	Exploring Ni(Mn <sub>1/3</sub> Cr <sub>2/3</sub> ) <sub>2</sub> O <sub>4</sub> spinel-based electrodes for solid oxide cells. Journal of Materials Chemistry A, 2020, 8, 3988-3998.	10.3	27
131	High-Temperature Electrochemical Devices Based on Dense Ceramic Membranes for CO2 Conversion and Utilization. Electrochemical Energy Reviews, 2021, 4, 518-544.	25.5	27
132	Silverâ€coated copper nanowires with improved antiâ€oxidation property as conductive fillers in Iowâ€density polyethylene. Canadian Journal of Chemical Engineering, 2013, 91, 630-637.	1.7	26
133	Developing a Thermal- and Coking-Resistant Cobalt–Tungsten Bimetallic Anode Catalyst for Solid Oxide Fuel Cells. ACS Catalysis, 2016, 6, 4630-4634.	11.2	26
134	Toward highly efficient in situ dry reforming of H <sub>2</sub> S contaminated methane in solid oxide fuel cells via incorporating a coke/sulfur resistant bimetallic catalyst layer. Journal of Materials Chemistry A, 2016, 4, 9080-9087.	10.3	26
135	Understanding the Roles of Electrogenerated Co <sup>3+</sup> and Co <sup>4+</sup> in Selectivity‶uned 5â€Hydroxymethylfurfural Oxidation. Angewandte Chemie, 2021, 133, 20698-20705.	2.0	25
136	Fabrication of bi-layered proton conducting membrane for hydrocarbon solid oxide fuel cell reactors. Electrochimica Acta, 2010, 55, 1145-1149.	5.2	24
137	Corrosion Mechanisms and Materials Selection for the Construction of Flue Gas Component in Advanced Heat and Power Systems. Industrial & Engineering Chemistry Research, 2017, 56, 14141-14154.	3.7	24
138	Electrochemical oxidation of sour natural gas over La0.4Ce0.6O1.8–La0.4Sr0.6TiO3±Î′ anode in SOFC: A mechanism study of H2S effects. Applied Catalysis B: Environmental, 2015, 176-177, 627-636.	20.2	23
139	Co <sub>2</sub> CrO <sub>4</sub> Nanopowders as an Anode Catalyst for Simultaneous Conversion of Ethane to Ethylene and Power in Proton-Conducting Fuel Cell Reactors. Journal of Physical Chemistry C, 2018, 122, 4165-4171.	3.1	23
140	Investigation on the flow-induced corrosion and degradation behavior of underground J55 pipe in a water production well in the Athabasca oil sands reservoir. Journal of Petroleum Science and Engineering, 2019, 182, 106325.	4.2	23
141	Characterization and corrosion behavior of electroless Ni-Mo-P/Ni-P composite coating in CO2/H2S/Clâ^' brine: Effects of Mo addition and heat treatment. Surface and Coatings Technology, 2020, 403, 126416.	4.8	23
142	Insights into the erosion-enhanced corrosion on electroless Ni–P coating from single particle impingement. Corrosion Science, 2020, 166, 108422.	6.6	22
143	Cogeneration of ethylene and electricity in symmetrical protonic solid oxide fuel cells based on a La <sub>0.6</sub> Sr <sub>0.4</sub> Fe <sub>0.8</sub> Nb <sub>0.1</sub> Cu <sub>0.1</sub> O <sub>3â^î^</sub> electrode. Journal of Materials Chemistry A, 2020, 8, 25978-25985.	10.3	22
144	Strengthening absorption ability of Co–N–C as efficient bifunctional oxygen catalyst by modulating the d band center using MoC. Green Energy and Environment, 2023, 8, 459-469.	8.7	22

#	Article	IF	CITATIONS
145	Semiconductivity Conversion of Passive Films on Alloy 800 in Chloride Solutions Containing Various Concentrations of Thiosulfate. Journal of the Electrochemical Society, 2015, 162, C482-C486.	2.9	21
146	High Performance Tubular Solid Oxide Fuel Cell Based on Ba <sub>0.5</sub> Sr <sub>0.5</sub> Ce <sub>0.6</sub> Zr <sub>0.2</sub> Gd <sub>0.1</sub> Y <sub>0.1</sub> Conducting Electrolyte. Journal of the Electrochemical Society, 2018, 165, F764-F769.	O< <b>su</b> b>3-Î	° <b ₂ub>Proto
147	Thermally stable and coking resistant CoMo alloy-based catalysts as fuel electrodes for solid oxide electrochemical cells. Journal of Materials Chemistry A, 2018, 6, 15377-15385.	10.3	21
148	Electrolysis of waste water containing aniline to produce polyaniline and hydrogen with low energy consumption. International Journal of Hydrogen Energy, 2020, 45, 22419-22426.	7.1	21
149	Corrosion of SS310 and Alloy 740 in high temperature supercritical CO2 with impurities H2O and O2. Corrosion Science, 2021, 184, 109350.	6.6	21
150	NiFe P@NiCo-LDH nanoarray bifunctional electrocatalysts for coupling of methanol oxidation and hydrogen production. International Journal of Hydrogen Energy, 2022, 47, 17150-17160.	7.1	21
151	Regulating the Electron Localization of Metallic Bismuth for Boosting CO2 Electroreduction. Nano-Micro Letters, 2022, 14, 38.	27.0	21
152	Minimum and well-dispersed platinum nanoparticles on 3D porous nickel for highly efficient electrocatalytic hydrogen evolution reaction enabled by atomic layer deposition. Applied Surface Science, 2019, 494, 1091-1099.	6.1	20
153	Influence of H2S on the general corrosion and sulfide stress cracking of pipelines steels for supercritical CO2 transportation. Corrosion Science, 2021, 190, 109639.	6.6	20
154	Zr <sub>2</sub> N <sub>2</sub> O Coating-Improved Corrosion Resistance for the Anodic Dissolution Induced by Cathodic Transient Potential. ACS Applied Materials & Interfaces, 2018, 10, 40111-40124.	8.0	19
155	Unlocking the impurity-induced pipeline corrosion based on phase behavior of impure CO2 streams. Corrosion Science, 2020, 165, 108367.	6.6	19
156	LaCrO3â^'VOxâ^'YSZ Anode Catalyst for Solid Oxide Fuel Cell Using Impure Hydrogen. Journal of Physical Chemistry C, 2007, 111, 16679-16685.	3.1	18
157	Passivity degradation of alloy 800 in simulated crevice chemistries. Transactions of Tianjin University, 2015, 21, 234-243.	6.4	18
158	Standalone Solar Carbon-Based Fuel Production Based on Semiconductors. Cell Reports Physical Science, 2020, 1, 100101.	5.6	18
159	Novel folic acid complex derived nitrogen and nickel co-doped carbon nanotubes with embedded Ni nanoparticles as efficient electrocatalysts for CO <sub>2</sub> reduction. Journal of Materials Chemistry A, 2020, 8, 5105-5114.	10.3	18
160	Co- and N-doped carbon nanotubes with hierarchical pores derived from metal–organic nanotubes for oxygen reduction reaction. Journal of Energy Chemistry, 2021, 53, 49-55.	12.9	18
161	Microfabrication of the Ammonia Plasma-Activated Nickel Nitride–Nickel Thin Film for Overall Water Splitting in the Microfluidic Membraneless Electrolyzer. ACS Applied Energy Materials, 2021, 4, 9639-9652.	5.1	18
162	Directionally maximizing CO selectivity to near-unity over cupric oxide with indium species for electrochemical CO2 reduction. Chemical Engineering Journal, 2022, 427, 131654.	12.7	18

#	Article	IF	CITATIONS
163	Insights into the Electrochemical Corrosion Behavior and Mechanism of Electroless Ni-P Coating in the CO2/H2S/Clâ <sup>~?</sup> Environment. Corrosion, 2020, 76, 578-590.	1.1	18
164	Near-Neutral pH Stress Corrosion Cracking Susceptibility of Plastically Prestrained X70 Steel Weldment. Metallurgical and Materials Transactions A: Physical Metallurgy and Materials Science, 2010, 41, 2538-2547.	2.2	17
165	In-situ exsolved FeNi nanoparticles on perovskite matrix anode for co-production of ethylene and power from ethane in proton conducting fuel cells. Electrochimica Acta, 2021, 393, 139096.	5.2	17
166	Accelerating photoelectric CO2 conversion with a photothermal wavelength-dependent plasmonic local field. Applied Catalysis B: Environmental, 2021, 298, 120533.	20.2	17
167	Densely packed ultrafine SnO2 nanoparticles grown on carbon cloth for selective CO2 reduction to formate. Journal of Energy Chemistry, 2022, 71, 159-166.	12.9	17
168	Effect of substitution of B-sites by Mn, Fe and Co in double perovskite-type Ba3CaNb2O9 on structure and electrical properties. RSC Advances, 2013, 3, 23824.	3.6	16
169	Exploring MnCr2O4–Gd0.1Ce0.9O2-δas a composite electrode material for solid oxide fuel cell. International Journal of Hydrogen Energy, 2019, 44, 31333-31341.	7.1	16
170	Energyâ€saving H <sub>2</sub> Generation Coupled with Oxidative Alcohol Refining over Bimetallic Phosphide Ni <sub>2</sub> Pâ^'CoP Junction Bifunctional Electrocatalysts. ChemSusChem, 2021, 14, 5450-5459.	6.8	16
171	Generating C4 Alkenes in Solid Oxide Fuel Cells via Cofeeding H <sub>2</sub> and <i>n</i> -Butane Using a Selective Anode Electrocatalyst. ACS Applied Materials & Interfaces, 2020, 12, 16209-16215.	8.0	15
172	CO2 emission free co-generation of energy and ethylene in hydrocarbon SOFC reactors with a dehydrogenation anode. Physical Chemistry Chemical Physics, 2011, 13, 19615.	2.8	14
173	Highly cost-effective and sulfur/coking resistant VO <sub>x</sub> -grafted TiO <sub>2</sub> nanoparticles as an efficient anode catalyst for direct conversion of dry sour methane in solid oxide fuel cells. Journal of Materials Chemistry A, 2015, 3, 23973-23980.	10.3	14
174	The surface evolution of La0.4Sr0.6TiO3+ $\hat{l}'$ anode in solid oxide fuel cells: Understanding the sulfur-promotion effect. Journal of Power Sources, 2017, 343, 127-134.	7.8	14
175	Multiple-doped barium cerate proton-conducting electrolytes for chemical-energy cogeneration in solid oxide fuel cells. International Journal of Hydrogen Energy, 2018, 43, 19704-19710.	7.1	14
176	Core–Shell Structured Cu(OH) <sub>2</sub> @NiFe(OH) <sub><i>x</i></sub> Nanotube Electrocatalysts for Methanol Oxidation Based Hydrogen Evolution. ACS Applied Nano Materials, 2021, 4, 8723-8732.	5.0	14
177	Electrochemically reconstructed perovskite with cooperative catalytic sites for CO2-to-formate conversion. Applied Catalysis B: Environmental, 2022, 306, 121101.	20.2	14
178	1â€D dynamic modeling of SOFC with analytical solution for reacting gasâ€flow problem. AICHE Journal, 2008, 54, 1537-1553.	3.6	13
179	A mechanistic study of sulfur-induced passivity degradation of Alloy 800 in a simulated alkaline crevice environment at 300 ŰC. Journal of Solid State Electrochemistry, 2015, 19, 3567-3578.	2.5	13
180	Oxygen Evolution Reaction: Core–Shell Structured NiFeSn@NiFe (Oxy)Hydroxide Nanospheres from an Electrochemical Strategy for Electrocatalytic Oxygen Evolution Reaction (Adv. Sci. 10/2020). Advanced Science, 2020, 7, 2070052.	11.2	13

#	Article	IF	CITATIONS
181	Understanding the immobilization mechanisms of hazardous heavy metal ions in the cage of sodalite at molecular level: A DFT study. Microporous and Mesoporous Materials, 2020, 306, 110409.	4.4	13
182	Amorphous cobalt hydroxysulfide nanosheets with regulated electronic structure for high-performance electrochemical energy storage. Science China Materials, 2020, 63, 2303-2313.	6.3	13
183	Hydrogen generation and utilization in a two-phase flow membraneless microfluidic electrolyzer-fuel cell tandem operation for micropower application. Applied Energy, 2022, 305, 117945.	10.1	13
184	Surface Interactions between Water-in-Oil Emulsions with Asphaltenes and Electroless Nickel–Phosphorus Coating. Langmuir, 2020, 36, 897-905.	3.5	12
185	Role of Ca2+ in the CO2 corrosion behavior and film characteristics of N80 steel and electroless Ni–P coating at high temperature and high pressure. Materials Chemistry and Physics, 2021, 267, 124618.	4.0	12
186	Electrochemical behavior of CoCrMo implant in Ringer's solution. Surface and Interface Analysis, 2013, 45, 1323-1328.	1.8	11
187	Preparation and characterization of an solid oxide fuel cell tubular cellÂfor direct use with sour gas. Journal of Power Sources, 2013, 240, 411-416.	7.8	11
188	Improved coking resistance of direct ethanol solid oxide fuel cells with a Ni–Sx anode. Journal of Power Sources, 2014, 250, 212-219.	7.8	11
189	Promoting Influence of Doping Indium into BaCe <sub>0.5</sub> Zr <sub>0.3</sub> Y <sub>0.2</sub> O <sub>3â€î´</sub> as Solid Proton Conductor. International Journal of Applied Ceramic Technology, 2015, 12, 1174-1183.	2.1	11
190	Fouling mechanisms of asphaltenes and fine solids on bare and electroless nickel-phosphorus coated carbon steel. Fuel, 2019, 252, 188-199.	6.4	11
191	Probing the Interaction Mechanism between Oil-in-Water Emulsions and Electroless Nickel–Phosphorus Coating with Implications for Antifouling in Oil Production. Energy & Fuels, 2019, 33, 3764-3775.	5.1	11
192	Nanoalloy libraries from laser-induced thermionic emission reduction. Science Advances, 2022, 8, eabm6541.	10.3	11
193	Pitting susceptibility of induction-quenched pipeline with microstructural heterogeneity. Journal of Materials Science, 2012, 47, 6823-6834.	3.7	10
194	Co-generation of energy and ethylene in hydrocarbon fueled SOFCs with Cr3C2 and WC anode catalysts. Ceramics International, 2014, 40, 11781-11786.	4.8	10
195	Hydrogen-enhanced Surface Reactivity of X80 Pipeline Steel observed by Scanning Electrochemical Microscopy. Electrochemistry, 2016, 84, 238-242.	1.4	10
196	A bifunctional solid oxide electrolysis cell for simultaneous CO <sub>2</sub> utilization and synthesis gas production. Chemical Communications, 2016, 52, 13687-13690.	4.1	10
197	Rational design of CdCO3 nanoparticles decorated carbon nanofibers for boosting electrochemical CO2 reduction. Journal of Power Sources, 2021, 510, 230433.	7.8	10
198	Lessâ€Energy Consumed Hydrogen Evolution Coupled with Electrocatalytic Removal of Ethanolamine Pollutant in Saline Water over Ni@Ni <sub>3</sub> S <sub>2</sub> /CNT Nanoâ€Heterostructured Electrocatalysts. Small Methods, 2022, 6, e2101195.	8.6	10

#	Article	IF	CITATIONS
199	Formation of Hydroxyapatite Coating on Anodic Titanium Dioxide Nanotubes via an Efficient Dipping Treatment. Metallurgical and Materials Transactions A: Physical Metallurgy and Materials Science, 2011, 42, 3255-3264.	2.2	9
200	Nanoparticles as Anode Catalyst for Ethane Proton Conducting Fuel Cell Reactors to Coproduce Ethylene and Electricity. Advances in Physical Chemistry, 2011, 2011, 1-6.	2.0	9
201	"Revitalizing―degraded solid oxide fuel cells in sour fuels for bifunctional oxygen catalysis in zinc–air batteries. Green Chemistry, 2020, 22, 6075-6083.	9.0	9
202	Emerging anode materials architectured with NiCoFe ternary alloy nanoparticles for ethane-fueled protonic ceramic fuel cells. Journal of Power Sources, 2021, 515, 230634.	7.8	9
203	In-situ generated hydroxides realize near-unity CO selectivity for electrochemical CO2 reduction. Chemical Engineering Journal, 2022, 433, 133785.	12.7	9
204	Bariumâ€doped Sr <sub>2</sub> Fe <sub>1.5</sub> Mo <sub>0.5</sub> O <sub>6â€</sub> <i><sub>δ</sub></i> perovskite anode materials for protonic ceramic fuel cells for ethane conversion. Journal of the American Ceramic Society, 2022, 105, 3613-3624.	3.8	9
205	Interface modification of Ru-CeO2 co-infiltrated SFM electrode and construction of SDC/YSZ bilayer electrolyte for direct CO2 electrolysis. Electrochimica Acta, 2022, 426, 140771.	5.2	9
206	Title is missing!. Journal of Materials Science Letters, 2002, 21, 1195-1198.	0.5	8
207	Oxidation kinetics of copper nanowires synthesized by AC electrodeposition of copper into porous aluminum oxide templates. Journal of Materials Research, 2012, 27, 1755-1762.	2.6	8
208	Transient Potential Induced Anodic Dissolution of 316L Stainless Steel in Sulfuric Acid Solution. Journal of the Electrochemical Society, 2019, 166, C3355-C3363.	2.9	8
209	Corrosion performance of candidate boiler tube alloys under advanced pressurized oxy-fuel combustion conditions. Energy, 2021, 215, 119178.	8.8	8
210	Monitoring the Diffusion Layer During Passive Film Breakdown on Alloy 800 with Digital Holography. Acta Metallurgica Sinica (English Letters), 2015, 28, 1170-1174.	2.9	7
211	Effects of reduced sulfur on passive film properties of steam generator (SG) tubing: an overview. Anti-Corrosion Methods and Materials, 2019, 66, 317-326.	1.5	7
212	Stability of C3-C6 carbonium ions inside zeolites: A first principles study. Applied Surface Science, 2020, 503, 144148.	6.1	7
213	Perovskite Chromite With In-Situ Assembled Ni-Co Nano-Alloys: A Potential Bifunctional Electrode Catalyst for Solid Oxide Cells. Frontiers in Chemistry, 2020, 8, 595608.	3.6	7
214	Characterizing foulants on slotted liner and probing the surface interaction mechanisms in organic media with implication for an antifouling strategy in oil production. Fuel, 2021, 290, 120008.	6.4	7
215	Nonlinear state space modeling and simulation of a SOFC fuel cell. , 2006, , .		6
216	ZnS anchored on porous N, S-codoped carbon as superior oxygen reduction reaction electrocatalysts for Al-air batteries. Journal of Colloid and Interface Science, 2022, 609, 868-877.	9.4	6

#	Article	IF	CITATIONS
217	Generation of hydrogen accompanied with formate bifunctional NiCo P@NiCo-LDH nanosheet electrocatalyst. Journal of Alloys and Compounds, 2022, 906, 164305.	5.5	6
218	Impacts of catalyst, inorganic and organic corrodants on corrosion under batch-mode catalytic biomass hydrothermal liquefaction conversion. Corrosion Science, 2022, 204, 110409.	6.6	6
219	An investigation of fuel composition and flowâ€rate effects in a H <sub>2</sub> S fuelled sofc: Experiments and thermodynamic analysis. Canadian Journal of Chemical Engineering, 2012, 90, 1033-1042.	1.7	5
220	Lead-induced stress corrosion cracking behavior of mechanically surface-treated alloy 690. Materials Research Letters, 2016, 4, 180-184.	8.7	5
221	Influence of Major Operating Parameters (Temperature, Pressure, and Flow Rate) on the Corrosion of Candidate Alloys for the Construction of Hydrothermal Liquefaction Biorefining Reactors. Energy & Fuels, 2022, 36, 3134-3153.	5.1	5
222	Au/CeO <sub>2</sub> hollow nanospheres with enhanced catalytic activity for <scp>CO</scp> oxidation. International Journal of Applied Ceramic Technology, 2017, 14, 908-914.	2.1	4
223	Tuning the subsurface oxygen of Ag2O-derived Ag nanoparticles to achieve efficient CO2 electroreduction to CO. Electrochimica Acta, 2022, 403, 139656.	5.2	4
224	Memory effect and recoverability of passive film degradation of Alloy 800 in simulated crevice chemistry. Nuclear Engineering and Design, 2014, 280, 57-61.	1.7	3
225	Corrosion of duplex stainless steel 2205 in hot flue gas environments produced at advanced oxy-fired pressurized fluidized bed combustion plants. International Journal of Greenhouse Gas Control, 2020, 100, 103108.	4.6	3
226	Condensed phase corrosion of P91 and DSS 2205 steels at advanced oxygenâ€fired pressurized fluidized bed combustion plants. Materials and Corrosion - Werkstoffe Und Korrosion, 2021, 72, 757-771.	1.5	3
227	Solid-Liquid Mass Transfer under Flow Boiling Condition. Journal of the Electrochemical Society, 2016, 163, H618-H624.	2.9	2
228	Investigation of the Antifouling Mechanism of Electroless Nickel–Phosphorus Coating against Sand and Bitumen. Energy & Fuels, 2019, 33, 6350-6360.	5.1	2
229	High ionic conductivity of ultralow yttria concentration yttria-stabilized zirconia thin films. Journal of Vacuum Science and Technology A: Vacuum, Surfaces and Films, 2022, 40, 042405.	2.1	2
230	Fuel Cells: Anodeâ€Engineered Protonic Ceramic Fuel Cell with Excellent Performance and Fuel Compatibility (Adv. Mater. 40/2016). Advanced Materials, 2016, 28, 8921-8921.	21.0	1
231	Effect of interaction between two single-particle-impingements on the repassivation behavior of 304 stainless steel in a simulated groundwater. Corrosion Reviews, 2021, 39, 149-164.	2.0	1
232	Passivation degradation of Alloy 800 on nucleate boiling surface. Corrosion Engineering Science and Technology, 2017, 52, 391-396.	1.4	1
233	Lessâ€Energy Consumed Hydrogen Evolution Coupled with Electrocatalytic Removal of Ethanolamine Pollutant in Saline Water over Ni@Ni <sub>3</sub> S <sub>2</sub> /CNT Nanoâ€Heterostructured Electrocatalysts (Small Methods 3/2022). Small Methods, 2022, 6, .	8.6	1
234	Shape Effect of Zinc Nanostructures on Electrochemical CO <sub>2</sub> Reduction. ECS Meeting Abstracts, 2020, MA2020-02, 3877-3877.	0.0	1

#	Article	IF	CITATIONS
235	Fabrication and performance of PEN SOFCs with proton-conducting electrolyte. Frontiers of Chemical Engineering in China, 2007, 1, 40-44.	0.6	0
236	Guest editorial-fuel cells. Asia-Pacific Journal of Chemical Engineering, 2009, 4, 1-2.	1.5	0
237	Hierarchically Assembling Cobalt/Nickel Carbonate Hydroxide on Copper Nitride Nanowires for Highly Efficient Water Splitting. ECS Meeting Abstracts, 2021, MA2021-02, 1734-1734.	0.0	0
238	Electronic Regulation of Bismuth Oxide Via Sulfur Doping for Efficient CO2 Electroreduction to Formate. ECS Meeting Abstracts, 2021, MA2021-02, 824-824.	0.0	0
239	Steering the Selectivity of CuO to Near-Unity of CO with Indium Species for CO2 Electroreduction. ECS Meeting Abstracts, 2021, MA2021-02, 825-825.	0.0	0
240	Electrochemically Dismantled Perovskite with Cooperative Catalysis for CO2-to-Formate Conversion. ECS Meeting Abstracts, 2021, MA2021-02, 1318-1318.	0.0	0
241	Enhanced CO2 Adsorption Capability for Highly Selective Electroreduction of CO2 to Formate. ECS Meeting Abstracts, 2021, MA2021-02, 1740-1740.	0.0	0
242	Switchable CO <sub>2</sub> Electroreduction Induced By the Bismuth Moiety with Tunable Local Structures on Graphene. ECS Meeting Abstracts, 2022, MA2022-01, 2090-2090.	0.0	0
243	Tailoring a Three-Phase Microenvironment for High-Performance CO <sub>2</sub> Electroreduction. ECS Meeting Abstracts, 2022, MA2022-01, 1770-1770.	0.0	0